JOURNAL OF Materials CHEMISTRY

Structural, electro-magnetic and catalytic characterisation of the $LaMn_{1-x}Cu_xO_{3-\delta}$ system

Karel Knizek,[a,b] Marco Daturi[a,c] Guido Busca[c] and Claude Michel*[a]

[a] *Laboratoire CRISMAT-UMR-CNRS 6508, ISMRA et Université de Caen, 6, Bd Maréchal Juin, F-14050 Caen Cedex, France*

[b] *Institute of Physics ASCR, Cukrovarnicka 10, 162 53 Praha 6, Czech Republic*

[c] *Istituto di Chimica, Facoltà di Ingegneria, Università di Genova, Fiera del Mare, P.le J.F. Kennedy, I-16129 Genova, Italy*

The $LaMn_{1-x}Cu_xO_{3-\delta}$ system has been investigated for the first time from the point of view of the structure in relation to different preparation procedures. Skeletal FTIR spectroscopy has been used in support to XRD characterisation. Oxygen content, magnetic behaviour and resistivity have also been measured. Two compositions have been tested in the catalytic combustion of methane.

Introduction

The compound $LaMnO_3$ and its doped derivatives have been extensively investigated because of their magnetic properties. Electron hopping with spin memory provides a ferromagnetic double exchange interaction in $La_{1-x}Ca_xMnO_3$,[1] leading to canted ferromagnetic[2,3] or possibly helimagnetic[4] spin structures. Doped $LaMnO_3$ presents a colossal magnetoresistance due to the drastic increase of temperature during simultaneous ferromagnetic and insulator–metal transition by an applied field, and to the slight variation of structural parameters by rare earth ion substitution, which induces a monotonic change of transition temperature and an exponential variation of magnetoresistance.[5–10]

Furthermore, La–Mn–O perovskite oxides with high electric conductivity at high temperature in an oxidising atmosphere are considered to be some of the most promising cathode materials for solid state fuel cells.[11] This perovskite also presents interesting properties from the point of view of heterogeneous catalysis:[12,13] in particular $LaMnO_3$ has been envisaged as an active phase in the catalytic combustion of alkanes and alkenes.[14–17] Recently the substitution of Mn^{3+} by Mn^{4+} in perovskite-like compounds has been proposed in order to enhance the performance of such materials in CH_4 catalytic combustion at high temperature.[13,18–20] To obtain this result we have substituted a divalent cation at the B site of the perovskite. We have envisaged copper for this process because of its catalytic properties when inserted into these structures,[21,22] and since the oxidation state of copper (Cu^{2+}) is almost unchanged in these conditions[23] we avoid introducing a Cu^{2+}/Cu^{3+} ratio as an additional parameter. In the presence of manganese, copper is mainly Cu^{2+} in oxide systems, as shown by the existence of the spinel $Cu^{2+}Mn_2{}^{3+}O_4$[24] and of the perovskite-like compound $CaCu_3{}^{2+}Mn_4{}^{4+}O_{12}$ prepared in the presence of the oxidising $KClO_3$.[25] Furthermore, there has been very little investigation of the $LaMn_{1-x}Cu_xO_3$ solid solution, especially from the structural point of view.[23,26]

Modifications in various properties of La–Mn–O perovskite oxides, such as oxygen content and electric conductivity, are considered to be affected by the crystal structure changes induced by variation in Mn valence.[27] It is important to investigate the relation between the Mn valence and the crystal structure of this perovskite. In the present work we have studied the modifications that affect $LaMnO_3$ upon substitution of different percentages of Cu at the Mn site, and their effects on the catalytic activity.

Experimental

Samples of $LaMn_{1-x}Cu_xO_3$, with nominal composition $x=0$, 0.05, 0.10, 0.25, 0.50, 0.75, 0.90 and 0.95 have been prepared by solid state reaction and by solution chemistry.

In the first case we have again followed two methods of preparation: starting from La_2O_3, MnO_2 and CuO, we calcined the precursor powders at 1173 K for 24 h, then pressed the mixture into pellets fired at 1373 K for 40 h; finally the samples have been quenched at room temperature (r.t.) or cooled to r.t. at a low rate of *ca.* 45 K h^{-1}.

The samples prepared under mild conditions were obtained by dissolving stoichiometric amounts of $La(NO_3)_3\cdot 6H_2O$, $Cu(NO_3)_2\cdot 3H_2O$ and $Mn(CH_3CO_2)_2\cdot 4H_2O$, stirring them overnight and drying the solution at 393 K. The resulting solids were then calcined at 673 K, in order to decompose residual nitrates, and annealed at 1273 K for 5 h in air.

The degree of oxidation was determined by wet chemical analysis. The sample was dissolved under nitrogen flow and heating in HBr solution in the presence of Fe^{2+} ions, which are oxidised by $Mn^{3+,4+}$ and/or by Cu^{3+}. The remaining unreacted Fe^{2+} is determined by titration with $Ce(SO_4)_2$ using ferroin as indicator. DTA analyses were performed in a Setaram TG92 instrument, with a heating and cooling rate of 5 K min^{-1}. X-Ray diffraction spectra were collected in a Philips PW 1710 powder diffractometer (CuKα radiation, Ni filter, 35 kV, 35 mA). The data were analysed by the Rietveld method using the program FULLPROF.[28] IR spectra were recorded at room temperature with a Nicolet Magna 750 FTIR spectrometer (resolution 4 cm^{-1}) diluting the samples in KBr, for the near- and mean-IR region, or in polyethylene, for the far-IR region. The spectra have been treated using the Nicolet OMNIC℠ software. Magnetic measurements *vs.* temperature were performed in a magnetic field of 1.45 T using a vibrating sample magnetometer. Resistivity measurements have been carried out with the four point method, using direct current, in the temperature range between 5 and 300 K without applying any magnetic field.

Catalytic oxidation tests were performed in a quartz microreactor (id = 0.8 cm) filled with 0.45 g of finely ground catalyst powder ($d_p = 0.1$ μm). The reactor was fed with 1% CH_4 in air, and was operated under atmospheric pressure with GHSV = 54 000 N_{cc} $(g_{cat}\ h)^{-1}$ [N_{cc} = space velocity *vs.* gas flow rate in normal conditions (cc = cubic centimeters)]. The inlet and outlet gas compositions were determined by on line gas chromatography. A 4 m column (id = 5 mm) filled with Porapak QS was used to separate CH_4, CO_2 and H_2O with

He as carrier. One 3 m long molecular sieve (5 Å) column (id = 5 mm) was used for the separation and analysis of CO, N_2, O_2 and CH_4.

Results and Discussion

DTA measurements of $LaMn_{1-x}Cu_xO_3$ samples show exothermic peaks due to phase formation at around 1163 K, when the sample has been prepared *via* mild chemistry, and at around 1350 K if the reaction takes place after heating precursor mixed oxides. Furthermore this solid solution can crystallise in different space groups, according to preparation method. In the perovskite $LaMnO_3$ the Mn ions are surrounded by oxygen octahedra which share corners to form a three-dimensional MnO_3 network, while La occupies the space between these octahedra; La is too small to fill the space in the three-dimensional MnO_3 network, leading to a structural distortion. In general the flexibility of the perovskite structure enables a wide range of tolerance factor values, allowing various chemical substitutions and oxygen contents.[6] At low temperature two stable phases exist: the rhombohedral $LaMnO_{3.15}$ (JCPDS no. 32-0484), which is better described as $La_{0.95}Mn_{0.95}O_3$, and the orthorhombic $LaMnO_3$ phase (JCPDS no. 35-1353).

X-Ray characterisation

X-Ray diffraction analysis confirmed single phase formation for $x = 0$–0.5. In the samples with $x > 0.5$ the impurities La_2CuO_4 and CuO were found. Crystal symmetries and lattice parameters of the single-phase samples prepared by solid state reaction are reported in Table 1. The quenched samples are all orthorhombic (space group *Pbnm*), whereas the slowly cooled samples are rhombohedral ($R\bar{3}c$) for $x = 0$ and 0.05, and orthorhombic (*Pbnm*) for $x = 0.25$ and 0.50. The slowly cooled sample $x = 0.10$ is borderline between these structures and contains both orthorhombic and rhombohedral phases.

According to investigation of $La_{0.9}MnO_3$ by electron diffraction,[29] samples with apparent rhombohedral symmetry ($R\bar{3}c$) are in fact monoclinic (space group $I2/a$), but by powder XRD we cannot distinguish these two cases. Therefore we maintained $R\bar{3}c$ symmetry for these samples. For comparison the normalised volume, obtained by dividing by the number of formula units Z is included in Table 1, since Z is different for space group *Pbnm* ($Z = 4$) and $R\bar{3}c$ ($Z = 6$).

Chemical analysis only determines overall oxidation state and not the distribution of charge among cations, namely between Cu and Mn. We tentatively considered the charge distribution between Cu and Mn in the form $M_{1-2x}{}^{3+}Mn_x{}^{4+}Cu_x{}^{2+}$, thus calculating the valences of manganese listed in Table 2. This distribution seems reasonable taking in account the fact that divalent copper coexists with trivalent and tetravalent manganese in oxides.[24,25] We observed an effect similar to that of substitution of M^{2+} for RE in isostructural manganite perovskites (*e.g.* Ca^{2+}, Sr^{2+}, Ba^{2+} for Pr^{3+} [30–32]): the Mn valence in samples with $x = 0$ is higher than expected for ideal stoichiometry (probably due to La^{3+} vacancies). That of samples with x close to the solution limit is also lower (due to O^{2-} vacancies). The slowly cooled samples are more oxygenated than the quenched counterparts.

Table 1 Crystallographic data of the samples prepared by solid state reaction; (*a*) quenched samples, (*b*) slowly cooled samples

		lattice parameters/Å				
space group	x	a	b	$c/\sqrt{2}$	c	(V/Z)/Å^3
(*a*)						
Pbnm	0	5.541	5.514	5.513	7.797	59.6
Pbnm	0.05	5.538	5.514	5.515	7.799	59.5
Pbnm	0.10	5.539	5.517	5.518	7.804	59.6
Pbnm	0.25	5.538	5.515	5.518	7.804	59.6
Pbnm	0.50	5.530	5.493	5.506	7.787	59.1
(*b*)						
$R\bar{3}c$	0	5.532	5.532		13.343	58.9
$R\bar{3}c$	0.05	5.533	5.533		13.337	58.9
$R\bar{3}c$	0.10	5.534	5.534		13.329	58.9
Pbnm	0.10	5.535	5.490	5.499	7.777	59.1
Pbnm	0.25	5.531	5.491	5.501	7.779	59.1
Pbnm	0.50	5.531	5.492	5.503	7.782	59.1

Table 2 Mn valence determined by chemical analysis assuming Cu^{2+} and La^{3+}

x	quenched	slowly cooled	theoretical for $\delta = 0$
0	3.11	3.18	3
0.25	3.31	3.40	3.33
0.5	3.67	3.79	4

According to the heat treatment (quenched/slowly cooled) and symmetry (*Pbnm*/$R\bar{3}c$) the samples could be divided into three groups with constant normalised cell volume V/Z. The quenched sample with $x = 0.5$ is an exception, as discussed further.

(*a*) Slowly cooled samples of $R\bar{3}c$ symmetry for $x = 0$–0.10, where $V/Z = 58.9$ Å^3.

(*b*) Slowly cooled samples of *Pbnm* symmetry for $x = 0.10$–0.25 and also quenched sample $x = 0.5$, for which $V/Z = 59.1$ Å^3.

(*c*) Quenched samples of *Pbnm* symmetry for $x = 0$–0.25, for which $V/Z = 59.6$ Å^3.

The cell volume was observed to be independent of x. It could be qualitatively explained to agree with the assumed charge distribution $Mn_{1-2x}{}^{3+}Mn_x{}^{4+}Cu_x{}^{2+}$. In this case, substitution of Cu^{2+} for Mn also creates one Mn^{4+} from Mn^{3+} and the average size of Cu^{2+} and Mn^{4+} is comparable to that of Mn^{3+}. Combining Cu^{3+} and Mn^{3+} should decrease the average ionic radii ($Cu^{2+} = 0.73$ Å, $Cu^{3+} = 0.54$ Å, $Mn^{3+} = 0.645$ Å, $Mn^{4+} = 0.53$ Å in sixfold co-ordination[33]).

The volume of quenched samples is greater since they contain less oxygen, *i.e.* more Mn^{3+}, which is larger than Mn^{4+}. The lower content of oxygen in quenched samples was confirmed by chemical analysis for $x = 0$, 0.25 and 0.5 (Table 2). Exceptions are the samples with $x = 0.5$: the volume of both is the same although they also have different oxygen content. This may be because in this case the volume is predominantly determined by Cu^{2+} which occupies 50% of the octahedral sites and the different content of Mn^{3+} and Mn^{4+} becomes less significant.

The samples prepared *via* mild chemistry belong to the *Pbnm* space group, having been calcined at 1273 K, with a heating and cooling rate of 10 K min^{-1}, which corresponds to a fast cooling, *i.e.* to quenching. Also the cell parameters are in line with the results presented above. Fig. 1 shows the experimental X-ray diffraction pattern of $LaMn_{0.5}Cu_{0.5}O_3$ powder calcined at 1273 K for 5 h and the calculated pattern for the *Pbnm* space group. It is important to point out that the sample is almost pure. Some compositions with $x > 0.5$ have also been tested, but they always gave triphasic samples, containing the limiting solid solution, La_2CuO_4 and CuO.

FTIR spectroscopy

Fig. 2 shows the FTIR skeletal spectra of samples with $x = 0.5$ and $x = 0.9$ in comparison with pure $LaMnO_3$ and La_2CuO_4. According to the factor group analysis, the irreducible representation (Γ_{opt}) for the optical modes of the orthorhombic phase ($D_{2h}{}^{16}$ space group) is $\Gamma_{opt} = 7A_g(R) + 7B_{1g}(R) + 5B_{2g}(R) + 5B_{3g}(R) + 8A_u(\text{inactive}) + 7B_{1u}(IR) + 9B_{2u}(IR) + 9B_{3u}(IR)$ while for the rhombohedral phase ($D_{3d}{}^6$ space group) $\Gamma_{opt} = A_{1g}(R) + 3A_{2g}(\text{inactive}) + 4E_g(R) + 2A_{1u}(\text{inactive}) + 3A_{2u}(IR) + 5E_u(IR)$.

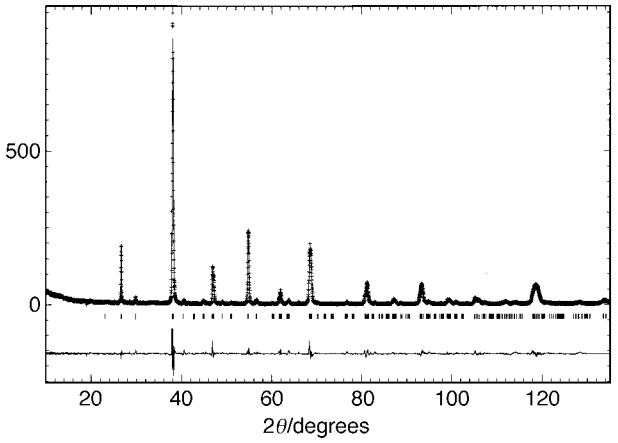

Fig. 1 Experimental (+), calculated (—) and difference XRD diffraction patterns of the sample $LaMn_{0.50}Cu_{0.50}O_3$ prepared *via* solution chemistry. Space group *Pbnm*, $R_i = 6.60\%$.

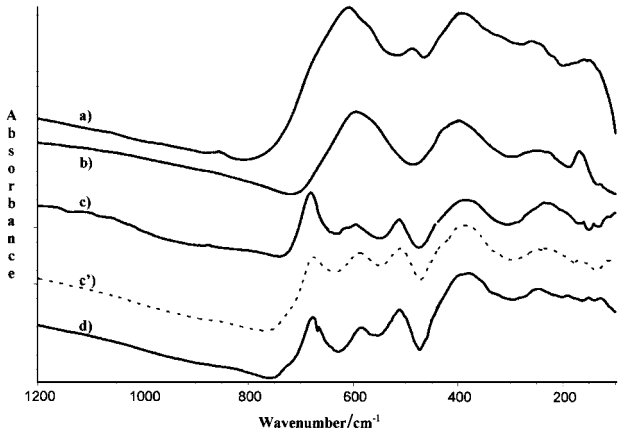

Fig. 2 FTIR/FTFIR spectra of samples $LaMnO_3$ (a), $LaMn_{0.50}Cu_{0.50}O_3$ (b), $LaMn_{0.10}Cu_{0.90}O_3$ (c) and La_2CuO_4 (d). (c′) represents a simulated spectrum of sample $LaMn_{0.10}Cu_{0.90}O_3$ starting from the linear combination of spectra (a) and (d).

The sample with $x=0$ (Fig. 2a) presents a strong band in the Mn–O–Mn stretching region, weakly split at 608 and 570 cm^{-1}, evident bands at 480, 395 and 259 cm^{-1} and more than one component in the range 180–150 cm^{-1}. According to the interpretation of different perovskite phase spectra, the first absorption arises from the ν_3 IR active vibrational mode of the perfect octahedral species MnO_6 (F_{1u}), which is in fact essentially an asymmetric Mn–O–Mn stretch. The origin of its splitting is the loss of degeneracy upon lowering the symmetry of the octahedron and the increase of the unit cell to more than one ABO_3 unit. In the region 450–250 cm^{-1} we expect the modes arising from the deformations of the MnO_6 octahedra (ν_4, F_{1u}, IR active and ν_6, F_{2u}, inactive). These modes give rise to three IR-active bands for the rhombohedral phase ($A_{2u}+2E_u$) and to nine IR-active modes for the orthorhombic phase ($3B_{1u}+3B_{2u}+3B_{3u}$). In the low frequency region the bands arising from the La vibrational mode are expected.[34]

In general, the spectrum of our sample appears broad and poorly defined, when compared with those of stoichiometric $LaFeO_3$ and $LaCrO_3$ which we have previously studied.[34] The splitting of the higher frequency band and the low complexity of the MnO_6 octahedra deformation range are more in line with the rhombohedral oxygen-rich structure (eight IR bands expected) than with the orthorhombic stoichiometric structure (25 IR bands expected). However, it seems clear that the broadening of IR bands, doubtless associated to a random non-stoichiometry, could mask the complexity of the spectra. Furthermore we must take into account that vibrational spectroscopy is in fact more sensitive than X-ray diffraction, as shown previously;[35,36] thus small amounts of impurities or mixed phases can be more clearly observed. Consequently, the coexistence or intergrowth of orthorhombic and rhombohedral phases cannot be excluded. We may thus assume that our rapidly cooled sample appears orthorhombic (*i.e.* oxygen poor) in the core of the grains (detectable by XRD), and covered by a rhombohedral film, accessible to oxygen even during the quench. Then the phase transition reduces to a problem of O_2 diffusivity, *i.e.* a kinetic phenomenon. The sample with $x=0.5$ (Fig. 2b) shows almost the same features as pure $LaMnO_3$, with a further band broadening, as generally found in random solid solution IR spectra,[37] and a small peak shift towards lower frequencies, possibly due to the substitution of heavier copper for manganese.

Fig. 2d shows the IR spectrum of La_2CuO_4, belonging to the orthorhombic $D_{2h}{}^{18}$ space group, which gives rise to the following irreducible representation: $\Gamma_{opt}=5A_g(R)+3B_{1g}(R)+4B_{2g}(R)+6B_{3g}(R)+4A_u(\text{inactive})+6B_{1u}(IR)+7B_{2u}(IR)+4B_{3u}(IR)$.

These modes have been assigned to $[CuO_2]_n$ sheets, Cu—O apical stretching and La (lattice) vibrations. In particular the sharp band at 690 cm^{-1} can be attributed to the stretching/bending mode of the in-plane Cu—O bonds.[38]

Note that the spectrum of the $LaMn_{0.1}Cu_{0.9}O_3$ sample (Fig. 2c) is due to the linear combination of $LaMnO_3$ and La_2CuO_4 spectra, each multiplied by a factor that takes into account the relative abundance of the single phase and the absorbance coefficient. Fig. 2c′ shows a tentative simulation of this spectrum taking 0.1 and 0.9 as coefficients respectively for $LaMnO_3$ and La_2CuO_4. The presence of unmixed CuO in the solid solution is also indicated by the band around 620 cm^{-1} which is absent in the simulated combination.

Magnetic measurements

Measurement of magnetic moment (μ) revealed ferromagnetic character for all samples. The Curie temperature T_C was defined as the temperature corresponding to the minimum of $dM/dT = f(T)$. T_C decreases from 160 K for the quenched $x=0$ sample, to 55 K for $x=0.5$ samples (Table 3). Magnetic moments mol^{-1} at helium temperature are reported in Table 3. For $x=0$ this is comparable to the expected moment for a ferromagnetic ordered material. For $x>0$ the moment and Curie transition temperature decrease concomitantly. Similar behaviour has been observed in $LaCr_xMn_{1-x}O_3$ materials.[39] In doped $La_{1-x}A_xMnO_3$ (A = Ba,Ca,Sr) assumed ferromagnetic (FM) interactions between Mn^{3+}–Mn^{3+} or Mn^{3+}–Mn^{4+} and antiferromagnetic (AFM) interaction between Mn^{4+}–

Table 3 Magnetic moment mol^{-1} (μ_{He}) at $T=5$ K, estimated Curie temperature T_C, resistivity at room temperature and activation energy of conductivity E_A; (*a*) quenched samples, (*b*) slowly cooled samples

				E_A/eV	
x	μ_{He} ($T=5$ K)/μ_B	T_C/K	R/Ω m	r.t.	below T_C
(*a*)					
0	3.47	160	0.05	0.14	0.108
0.1	3.01	130	0.03	0.14	0.117
0.25	1.36	90	0.02	0.14	—[a]
0.5	0.26	55	0.03	0.13	—[b]
(*b*)					
0	3.10	150	0.02	0.14	0.082
0.1	2.06	110	0.02	0.14	0.12
0.25	0.57	75	0.01	0.14	—[a]
0.5	0.26	55	0.01	0.11	—[b]

[a]Not determined because the resistance was too high to be measured by our system. [b]Continuously decreases with temperature.

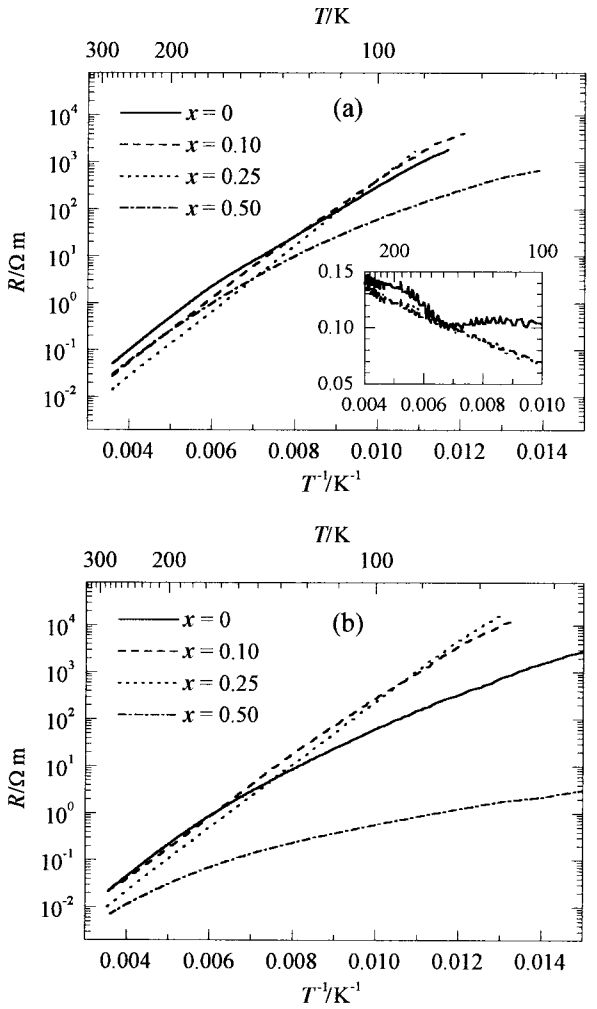

Fig. 3 Resistivity on a semilogarithmic scale *vs.* temperature of quenched (a) and slowly cooled (b) samples. Inset shows the value of the derivative of $\log(R)/\mathrm{d}T^{-1}$ *vs.* T^{-1} for $x=0$ (upper) and 0.5 (lower).

Mn^{4+} [40,41] occur. Substitution of Cu in Mn sites leads to strong Cu^{2+}–Cu^{2+} AFM interactions. Increasing the copper content also increases the Mn^{4+} amount (Table 2) and consequently the influence of the AFM interactions on the magnetic moment and a lowering of the ferromagnetic ordering results.

Electrical properties

Resistivity measurements are plotted in Fig. 3 and resistivity at room temperature and activation energies are reported in Table 3. The data for samples $x=0$–0.25 are typical for activated conductivity. The measured temperature range could be divided into three regions. In the first around room temperature, the activation energy is $E_A \approx 0.14$ eV. Note that this value is close to that observed in $LaCr_xMn_{1-x}O_3$ samples,[39] $E_A=$ 0.11–0.12 eV. In the second region starting about 50 K above T_C a linear decrease of E_A is observed to a new constant value in the third region [see example for $x=0$ in the inset of Fig. 3]. The appearance of resistivity is different for $x=0.5$, for which the slope of the curve $\log R=f(1/T)$ decreases continuously and the formula for activated conductivity cannot be applied. Thus the reported E_A for this sample should be considered as simply as a value of the slope rather than the activation energy. This might be attributed to a possible small amount of copper in the Cu^{3+} oxidation state, conferring an admixture of metallic conductivity to the sample, which is characteristic of $LaCuO_3$.

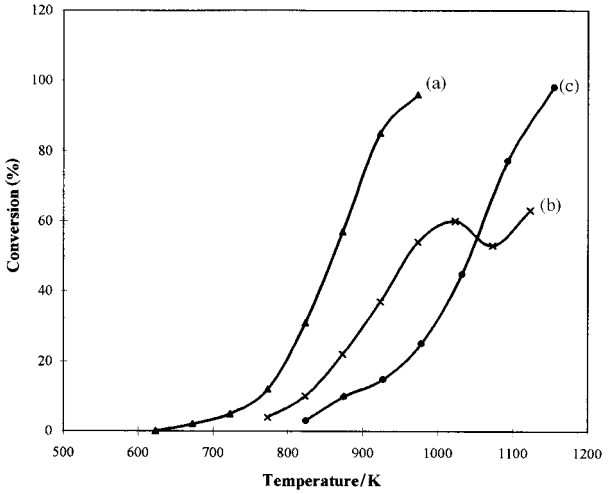

Fig. 4 Oxidation of methane on $LaMnO_3$ annealed at 973 K (a), on $LaMnO_3$ annealed at 1373 K (b) and on $LaMn_{0.5}Cu_{0.5}O_3$ annealed at 1273 K (c)

Catalytic properties

The solid solution $LaMn_{1-x}Cu_xO_3$ has already been studied from the point of view of catalytic combustion, but the tentative application to low temperature reactions caused it to be discarded because its activity is the lowest among the tested catalysts.[26,42] The very low surface area of the material due to the severe preparation conditions, certainly contributes to this inefficiency. We thus consider applying this material to a field where its specific properties would be appropriate, *e.g.* high temperature catalytic combustion.

The samples $LaMnO_3$ (calcinated at 773 and 1373 K) and $LaMn_{0.5}Cu_{0.5}O_3$ have been tested in the catalytic combustion of methane. As already reported elsewhere,[17,18] $LaMO_3$ perovskites (M = transition element) are active phases in the catalytic combustion of CH_4, CO and H_2, with performances comparable with other routinely used catalysts, such as supported noble metals, or new phases like hexa-aluminates.

Fig. 4 shows plots of CH_4 conversion *vs.* reaction temperature for the investigated system. $LaMnO_3$ calcined at 973 K presents a high activity at lower temperatures; conversely, if calcinated at 1373 K, its conversion performances decrease markedly and an anomalous behaviour is seen at increased reaction temperature. The reasons of such de-activation cannot be ascribed to the lowering of the material specific surface area, subsequent to the sintering phenomena, given that the conversion curve shape is totally reversible upon lowering the temperature; but rather are related to the variation in the degree of non-stoichiometry in $LaMnO_{3\pm\delta}$ at high temperature.[43]

Conversely sample $LaMn_{0.5}Cu_{0.5}O_4$ shows lower activity at lower temperatures, but a high stability even above 1100 K. The first phenomenon can be explained by the small value of the specific surface area ($\leqslant 1\ m^2\ g^{-1}$), while the second could be attributed to the increased redox stability of the copper containing phase, where the rôle of the Cu^{2+} substitution is correlated with the formation of more stable Mn^{4+} cations and with the fixation of the oxygen stoichiometry of the material.

Conclusion

The $LaMn_{1-x}Cu_xO_{3+\delta}$ system has been thoroughly investigated from the structural point of view for the first time. Because of the thermal treatment, the crystal structure of the various compositions can show substantial transformations, doubtless due to the oxygen kinetics, which requires a mini-

mum amount of time to reach the stoichiometric stability. This fact has been confirmed by IR measurements, that have demonstrated partial differences between surface and bulk system composition. Thermal treatment also induces a lowering in the Curie temperature of the samples which are all ferromagnetic.

The solid solution has been found to be active in the catalytic combustion of methane, with a lowering of the activity with respect to pure $LaMnO_3$, but with an increase of thermal stability at high temperatures. This can be correlated with the fixed valence state of manganese after copper doping giving rise to an enhanced oxygen content stability.

The authors sincerely acknowledge Prof. P. Forzatti and Dr. G. Groppi for their kind support in catalytic measurements and Prof. P. Hoggan for useful discussion and suggestions.

References

1 C. Zener, *Phys. Rev*., 1951, **82**, 403.
2 E. O. Wollan and W. C. Koehler, *Phys. Rev*., 1995, **100**, 545.
3 P.-G. de Gennes, *Phys. Rev*., 1960, **118**, 141.
4 J. Inoue and S. Maekawa, *Mater. Sci. Eng. B*, 1995, **31**, 193; *Phys. Rev. Lett*., 1995, **74**, 3407.
5 K. Chahara, T. Ohno, M. Kasai and Y. Kozono, *Appl. Phys. Lett*., 1993, **63**, 1990.
6 S.-W. Cheong, H. Y. Hwang, P. G. Radaelli, D. E. Cox, M. Marezio, B. Batlogg, P. Schiffer and A. P. Ramirez, *Proc. Physical Phenomena at High Magnetic Fields—II Conference*, Tallahassee, FL, May 6–9, 1995, World Scientific, Singapore.
7 J. M. D. Coey, M. Viret, L. Ranno and K. Ounadjela, *Phys. Rev. Lett*., 1995, **75**, 3910.
8 A. Urushibara, Y. Moritomo, T. Arima, A. Asamitsu, G. Kido and Y. Tokura, *Phys. Rev. B*, 1995, **51**, 14 103.
9 H. L. Ju, J. Gopalakrishnan, J. L. Peng, Q. Li, G. C. Xiong, T. Venkatesan and R. L. Greene, *Phys. Rev. B*, 1995, **51**, 6143.
10 R. Mahendiran, R. Mahesh, N. Rangavittal, S. K. Tiwari, A. K. Raychaudhuri, T. V. Ramakrishnan and C. N. R. Rao, *Phys. Rev. B*, 1996, **53**, 3348.
11 *Fuel Cell System*, ed. L. J. M. J. Blomen and M. N. Mugenva, Plenum Press, New York, 1993, p. 470.
12 L. G. Tejuca, J. L. G. Fierro and J. M. D. Tascon, *Adv. Catal*., 1989, **36**, 237.
13 T. Seiyama, *Catal. Rev. Sci. Eng*., 1992, **34**, 281.
14 T. Nitadori, S. Kurihara and M. Misono, *J. Catal*., 1986, **98**, 221.
15 K. Tabata and M. Misono, *Catal. Today*, 1990, **8**, 249.
16 P. E. Marti and A. Baiker, *Catal. Lett*., 1994, **26**, 71.
17 C. Cristiani, G. Groppi, P. Forzatti, E. Tronconi, G. Busca and M. Daturi, Comparison of perovskite and hexaaluminate-type catalysts for CO/H_2-fuelled gas turbine combustors, in *11th International Congress on Catalysis—40th Anniversary*, ed. J. W. Hightower, W. N. Delgass, E. Iglesia and A. T. Bell, *Stud. Surf. Sci. Catal*., 1996, **101**.
18 F. M. Zwinkels, S. G. Järas and P. G. Menon, *Catal. Rev.-Sci. Eng*., 1993, **35**, 319
19 N. Gunasekaran, S. Saddawi and J. J. Carberry, *J. Catal*., 1996, **159**, 107.
20 M. Daturi, G. Busca, G. Groppi and P. Forzatti, *Appl. Catal. B*, 1997, **12**, 325.
21 H. Yasuda, N. Mizuno and M. Misono, *J. Chem. Soc*., *Chem. Commun*., 1990, 1094.
22 S. Rajadurai, J. J. Carberry, B. Li and C. B. Alcock, *J. Catal*., 1991, **131**, 582.
23 M. L. Rojas, J. L. G. Fierro, L. G. Tejuca and A. T. Bell, *J. Catal*., 1990, **124**, 41.
24 M. Beley, L. Padel and J. C. Bernier, *Ann. Chim.* (*Paris*), 1979, **3**, 429.
25 J. Chenavas, J. C. Joubert, M. Marezio and B. Bochu, *J. Solid State Chem*., 1975, **14**, 25.
26 G. Bagnasco, P. Ciambelli, L. Lisi, G. Russo, M. Turco, S. DE Rossi, M. Faticanti, G. Minelli, I. Pettiti and P. Porta, *Proceedings of the TCC-97 Conference*, Giardini Naxos, Italy, 22–25/06/1997.
27 T. Yao, T. Ito and T. Kokubo, *J. Mater. Res*., 1995, **10**, 1079.
28 J. Rodriguez-Carvajal, *Collected Abstracts of Powder Diffraction Meeting*, ed. J. Galy, Toulouse, France, July 1990, p. 127.
29 A. Maignan, C. Michel, M. Hervieu and B. Raveau, *Solid State Commun*., 1997, **101**, 277.
30 Z. Jirák, S. Krupicka, Z. Šimša, M. Dlouhá and S. Vratislav, *J. Magn. Magn. Mater*., 1985, **53**, 153.
31 Z. Jirák, E. Pollert, A. F. Andersen, J.-C. Grenier and P. Hagenmuller, *Eur. J. Solid State Inorg. Chem*., 1990, **27**, 421.
32 K. Knízek, Z. Jirák, E. Pollert, F. Zounová and S. Vratislav, *J. Solid State Chem*., 1992, **100**, 292.
33 R. D. Shannon, *Acta Crystallogr*., *Sect. A*., 1976, **32**, 751.
34 M. Daturi, G. Busca and R. J. Willey, *Chem. Mater*., 1995, **7**, 2115.
35 G. Busca, V. Buscaglia, M. Leoni and P. Nanni, *Chem. Mater*., 1994, **6**, 955.
36 M. I. Baraton, G. Busca, M. C. Prieto, G. Ricchiardi and V. Sanchez Escribano, *J. Solid State Chem*., 1994, **112**, 9.
37 M. Daturi, G. Busca, M. M. Borel, A. Leclaire and P. Piaggio, *J. Phys. Chem. B*, 1997, **101**, 4358.
38 M. Daturi, G. Busca and M. Ferretti, *Nuovo Cimento Soc. Ital. Fis. D*, 1994, **16**, 1785.
39 R. Gundakaram, A. Arulraj, P. V. Vanitha, C. N. R. Rao, N. Gayathri, A. K. Raychaudhuri and A. K. Cheetam, *J. Solid State Chem*., 1996, **127**, 354.
40 G. H. Jonker, *Physica*, 1954, **20**, 1118; 1956, **22**, 707.
41 R. Gundakaram, A. Arulraj, P. V. Vanitha, C. N. R. Rao, N. Gayathri, A. K. Raychaudhuri and A. K. Cheetam, *J. Solid State Chem*., 1996, **127**, 354.
42 H.-G. Lintz and K. Wittstock, *Catal. Today*, 1996, **29**, 457.
43 J. A. M. Van Roosmalen, E. H. P. Cordfunke, R. B. Helmholdt and H. W. Zandbergen, *J. Solid State Chem.* 1994, **110**, 100.

Paper 8/01503A; *Received* 23*rd February*, 1998